Enhanced Sustainable Green Revolution Yield via Nitrogen-Responsive Chromatin Modulation in Rice

Kun Wu[1*], Shuansuo Wang[1*], Wenzhen Song[1,2], Jianqing Zhang[1,2], Yun Wang[1,2], Qian Liu[1], jianping Yu[1], Yafeng Ye[1,3], Shan Li[1,2], Jianfeng Chen[1,2], Ying Zhao[1,2], Jing Wang[1,2], Xiaokang Wu[1,2], Meiyue Wang[4], Yijing Zhang[4], Binmei Liu[3], Yuejin Wu[3], Nicholas P. Harberd[5]†, Xiangdong Fu[1,2]†

[1]*State Key Laboratory of Plant Cell and Chromosome Engineering, Institute of Genetics and Developmental Biology, Innovation Academy for Seed Design, Chinese Academy of Sciences, Beijing 100101, China*

[2]*College of Life Sciences, University of Chinese Academy of Sciences, Beijing, 100049, China*

[3]*Key laboratory of high magnetic field and Ion Beam Physical Biology, Hefei Institutes of Physical Science, Chinese Academy of Sciences, Hefei, Anhui 230031, China*

[4]*National Key Laboratory of Plant Molecular Genetics, CAS Center for Excellence in Molecular Plant Sciences, Shanghai Institute of Plant Physiology and Ecology, Shanghai Institutes for Biological Sciences, Chinese Academy of Sciences, Shanghai, 200032, China.*

[5]*Department of Plant Sciences, University of Oxford, South Parks Road, Oxford OX1 3RB, UK*

*These authors contributed equally to this work.

†Corresponding authors. Email: nicholas.harberd@plants.ox.ac.uk (N.P.H.);

xdfu@genetics.ac.cn (X.F.)

Because environmentally degrading inorganic fertilizer use underlies current worldwide cereal yields, future agricultural sustainability demands enhanced nitrogen use-efficiency. Here we discover that genome-wide promotion of histone H3 lysine 27 tri-methylation enables nitrogen stimulation of rice tillering: APETALA2-domain transcription factor NGR5 (NITROGEN-MEDIATED TILLER GROWTH RESPONSE 5) facilitates nitrogen-dependent recruitment of polycomb repressive complex 2 to repress branching-inhibitory genes. NGR5 is a target of gibberellin receptor GIBBERELLIN INSENSITIVE DWARF1 (GID1) promoted proteasomal destruction. DELLA proteins characterized by the presence of a conserved motif (aspartate-glutamate-leucine-leucine-alanine) competitively inhibit the GID1-NGR5 interaction and explain increased tillering of green revolution varieties. Increased NGR5 activity consequently uncouples tillering from nitrogen-regulation, boosting rice yield at low nitrogen fertilization levels. NGR5 thus enables enhanced nitrogen use-efficiency for improved future agricultural sustainability and food security.

The agricultural green revolution of the 1960's enhanced cereal crop yields, fed a growing world population, and was in part due to increased cultivation of semi-dwarf green revolution varieties (*1-4*). The beneficial semi-dwarfism is conferred by mutant alleles at the wheat *Reduced height-1* (*Rht-1*; *5*,*6*) and rice *Semi-Dwarf1* (*SD1*; *7*,*8*) loci that enhance the activity of growth-repressing DELLA proteins (DELLAs). Normally, the phytohormone gibberellin stimulates DELLAs destruction (*9*,*10*), thus promoting plant growth. However, the mutant wheat DELLA protein Rht-1 likely resists gibberellin-stimulated destruction (*5*), whilst the rice *sd1* allele reduces gibberellin abundance (*11*,*12*) and increases accumulation of the rice DELLA protein SLR1 (SLENDER RICE1; *13*). The result is plants that are shorter than normal, which, because they are shorter, are more resistant to lodging (the flattening of plants by wind and rain; *4*). However, green revolution rice varieties require a high nitrogen fertilizer supply to achieve maximum yield potential, and the drive toward increased agricultural sustainability has raised the profile of reducing nitrogen fertilizer use in green revolution rice varieties (*13*). Grain yield is the sum of the multiplicative integration of three major components (tiller numbers per plant, grain numbers per panicle and 1,000-grain weight; *14*), and an increased tillering ability in high-density planting conditions contributes to the high-yield properties of green revolution rice varieties (*1*,*15*). Further increase in tiller (lateral branch) numbers at low

nitrogen supply is therefore important for future agricultural sustainability, and a key cereal breeding goal. Here, we first define the mechanisms underlying the promotive effects of nitrogen on tiller bud outgrowth. We then show how genetic modulation of these mechanisms can enable increased grain yield of green revolution varieties despite reduced nitrogen input, thus advancing agricultural sustainability.

Nitrogen promotes rice tillering via NGR5

The tiller number per plant of *indica* rice variety Nanjing6 (NJ6) increases with increasing nitrogen supply (Fig. 1A). Additional effects of increasing nitrogen on NJ6 include increasing grain number (per panicle) and yield (per plant) (*13*; fig. S1A-C). NJ6-*sd1* (a NJ6 isogenic line containing the *sd1* allele) also displays nitrogen-dependent tiller number increases: increased tiller numbers per plant under different nitrogen fertilization levels, with tiller numbers being consistently higher in NJ6-*sd1* than in NJ6 (Fig. 1A). The *Rht-B1b* (formerly termed *Rht-1*) allele confers similar properties on wheat (versus the *Rht-B1a* control allele; Fig. 1B; fig. S1D-F). In contrast, either exogenous gibberellin treatment or overexpression of the rice gibberellin receptor GID1 (*16*) inhibits nitrogen-promoted tillering (fig. S2). Thus, the enhanced DELLA function typical of green revolution varieties increases nitrogen-induced promotion of tiller number. Further analysis showed that nitrogen-induced increases in tiller number in the elite *sd1*-containing *indica* rice variety 9311 (fig. S3A, B) are not due to nitrogen-responsive increases in numbers of lateral buds, but to increased numbers of buds initiating outgrowth and tiller branch extension (*17*; fig. S3C-E).

We next screened an ethyl-methane-sulphonate (EMS)-mutagenized 9311 population for mutants displaying an altered tiller number nitrogen-response. Amongst such mutants, *ngr5* (*nitrogen-mediated tiller growth response 5*) displays a reduced tiller number that is insensitive to changes in nitrogen supply (Fig. 1C, D). Map-based cloning (fig. S4A, B) and genetic complementation (Fig. 1C, D; fig. S4C, D) revealed the *NGR5* allele to encode an APETALA2 (AP2)-domain transcription factor (NGR5, previously known as SMOS1 (SMALL ORGAN SIZE1) and RLA1 (REDUCED LEAF ANGLE1); *18-20*), thus identifying an unknown function for NGR5 in nitrogen-responsive tillering regulation. The *ngr5* allele carries a G to A nucleotide substitution conferring a G to R amino acid residue substituted mutant protein (fig. S4B) which fails to complement *ngr5* phenotypes (fig. S4C-F). In addition to its effect on tiller number (Fig. 1C, D; fig. S4D), *NGR5* is required for nitrogen-induced promotion of panicle branching and grain number (fig. S4E, F). Accordingly, whilst 9311 grain yield per plot

increased progressively with increasing nitrogen supply (*13*), this effect was abolished in *ngr5* (fig. S4G). Further analysis showed that lack of NGR5 (in *ngr5*) has no effect on the formation of tiller buds (lateral bud initials; fig.S3C), but reduces the number of buds initiating lateral outgrowth and tiller branch extension (fig. S3D, E), thus confirming that nitrogen-responsive regulation of tillering is dependent upon *NGR5*.

We next found that an increasing nitrogen supply increases NGR5 abundance at both mRNA and protein levels (Fig. 1E, F). First, increasing nitrogen supply increases *NGR5* mRNA abundance, an effect abolished in *ngr5* (Fig. 1E). Second, whilst nitrogen supply has no effect on *NGR5-HA* (HA-tagged fusion gene) mRNA abundance in plants transgenically expressing *p35S::NGR5-HA* (fig. S5), accumulation of NGR5-HA fusion protein is coordinatedly up-regulated with increasing nitrogen supply (Fig. 1F). Furthermore, NGR5 positively regulates tillering over a wide expression range, because the *p35S::NGR5* transgene increases 9311 tiller number (thus mimicking the effect of increasing nitrogen supply on tillering capacity; Fig. 1G). We conclude that nitrogen promotes increase in NGR5 abundance, which in turn promotes tiller bud outgrowth. In addition, because *ngr5* suppresses the *sd1*-conferred tillering phenotype of 9311 (Fig. 1D), NGR5 is necessary for the DELLA-promoted increase in tiller number characteristic of green revolution varieties.

NGR5 represses branching inhibitor genes

RNA-sequencing analysis next revealed that lack of *NGR5* causes genome-wide change in mRNA abundance, with multiple differentially expressed genes displaying increase in mRNA abundance in *ngr5* (fig. S6A). Further gene set enrichment analysis revealed a correlation between genes up-regulated in *ngr5* and the set of H3K27me3 (histone H3 lysine 27 tri-methylation)-marked genes already known to be normally repressed by histone modification (fig. S6B), with H3K27me3-marking occurring at both TSS (transcription start site) and gene body regions of *ngr5* up-regulated genes (fig. S6C). These results suggest that NGR5 may be involved in PRC2 (polycomb repressive complex 2)-mediated epigenetic repression. Amongst genes up-regulated in *ngr5* (table S1), we identified *D14* (*Dwarf14*, encoding the receptor for the phytohormone strigolactone (SL); *21*), *D3* (*Dwarf3*, encoding the F-box component of the Skp, Cullin, F-box containing (SCF) ubiquitin ligase that targets the DWARF53 repressor of SL signaling for proteasomal destruction; *22-24*), *OsTB1* (*TEOSINTE BRANCHED1*, encoding a TCP domain transcription factor; *25*) and *OsSPL14* (*squamosa promoter binding protein-like-14*, encoding an SBP-domain transcription factor; *26*,*27*) genes all already known to inhibit

lateral branching and tiller number. qRT-PCR (quantitative real time polymerase chain reaction) analysis showed high nitrogen supply to reduce the abundances of mRNAs specified by these shoot branching inhibitor genes, and this effect was abolished by lack of *NGR5* function (in *ngr5*; fig. S6D). In addition, we found that lack of *D14* or *OsSPL14* function (conferred by *d14* or *osspl14* alleles; *28*,*29*) is epistatic to *ngr5* in regulating lateral branching (fig. S7). Thus, *D14* and *OsSPL14* function downstream of *NGR5*, and NGR5 mediates nitrogen-promoted increase in tiller number by repressing the inhibitory functions of *D14* and *OsSPL14* (and likely of other) branching regulatory genes.

Chromatin Immunoprecipitation-PCR (ChIP-PCR) experiments revealed binding of NGR5-HA to gene body and promoter regions of *D14* and *OsSPL14* (fig. S6E; confirmed in EMSA (electrophoretic mobility shift assays); fig. S6F). Furthermore, the extent and effect of binding on NGR5-target gene repression correlates with increasing nitrogen supply (fig. S6G, H). Whilst *D14* mRNA abundance reduces with increasing nitrogen supply in *NGR5* (but not in *ngr5*; fig. S6G), both extent of NGR5 binding and level of H3K27me3 modification at *D14* are correspondingly increased in a nitrogen-dependent manner (but not in *ngr5*; fig. S6G). Similar effects are observed for *OsSPL14* (fig. S6H), suggesting that NGR5 promotes tillering in response to increasing nitrogen supply by binding to target branching-inhibitory genes, thus causing their repression through regulation of H3K27me3 modification.

NGR5 recruits PRC2 for H3K27me3 deposition

To determine how NGR5 regulates nitrogen-promoted H3K27me3 modification, we first performed a yeast two-hybrid screen for NGR5 interactors, identifying LC2 (leaf inclination2, a component of the PRC2 complex; *30*) amongst many others (table S2). NGR5-LC2 interactions were confirmed in bimolecular fluorescence complementation (BiFC; Fig. 2A) and co-immunoprecipitation (Co-IP; Fig. 2B) experiments. Furthermore, a CRISPR (clustered regularly interspaced short palindromic repeats)/Cas9 (CRISPR-associated protein 9)-generated *LC2* reduced function allele (*lc2*; fig. S8A) was shown, like *ngr5*, to abolish nitrogen-promoted increase in tiller number (Fig. 2C, D). *lc2* also suppresses the increased tiller number conferred by *p35S::NGR5* (Fig. 1G; Fig. 2C, D), whilst lack of *D14* or *OsSPL14* function (conferred by *d14* or *osspl14*) is epistatic to *lc2* (fig. S9). Taken together, these results suggest that NGR5-dependent nitrogen-promoted increase in tiller number depends upon LC2 (PRC2 complex) function. Because PRC2 regulates genome-wide patterns of H3K27me3 methylation, we next conducted genome-wide surveys of H3K27me3 methylation in response

to varying nitrogen supply. Whilst increasing nitrogen supply alters genome-wide H3K27me3 methylation pattern, the extent of this alteration is reduced in *ngr5* (Fig. 2E), suggesting that nitrogen-mediated genome-wide reprogramming of H3K27me3 methylation is NGR5-dependent.

We next performed ChIP-sequencing experiments and identified a total of 453 binding sites shared in common by both NGR5 and LC2 (Fig. 2F; tables S3, S4). Further analysis identified potential target-site recognition motifs shared by both NGR5 and LC2 (Fig. 2G, H), with a predominant shared GCCGCC motif being common in the gene body regions of both *ngr5* up-regulated and nitrogen-induced genes (Fig. 2E). Accordingly, whilst increasing nitrogen supply progressively reduces *D14* and *OsSPL14* mRNA abundance in wild-type plants, these effects are abolished in *lc2* (Fig. 2I, J), just as they were in *ngr5* (fig. S6G, H). Furthermore, whilst increasing nitrogen supply progressively increases H3K27me3 modification of both *D14* and *OsSPL14* in wild-type plants, these effects are abolished in *lc2* (Fig. 2I, J). Taken together, these observations suggest that NGR5-driven recruitment of the PRC2 complex (of which LC2 is a component) to *D14* and *OsSPL14* results in repressive H3K27me3 modification of these genes in response to increased nitrogen supply, thereby promoting bud outgrowth and increasing tiller number.

NGR5 is a target of gibberellin receptor GID1

As shown above, nitrogen-induced increase in tiller number is enhanced in green revolution varieties (Fig. 1A, B), and this effect is inhibited by exogenous gibberellin treatment (fig. S2A). Analysis of both RNA-sequencing and ChIP-sequencing revealed multiple common gene targets to be co-regulated by NGR5 and gibberellin treatment (tables S5, S6). Furthermore, gibberellin treatment alters the change in genome-wide H3K27me3 modification pattern due to increasing nitrogen supply in a manner similar to the alteration conferred by *ngr5*, whilst a partially restored H3K27me3 modification pattern is induced by treatment with paclobutrazol (PAC, an inhibitor of gibberellin biosynthesis; Fig. 2E). In addition, gibberellin, like *ngr5* and *lc2*, inhibits the nitrogen-dependent increase in H3K27me3 modification and consequent repression of expression of shoot branching inhibitor genes such as *D14* (Fig. 2K) and *OsSPL14* (Fig. 2L). These observations suggest the existence of a mechanistic link between nitrogen- and gibberellin-mediated effects on tiller number.

In canonical gibberellin signalling, gibberellin binds its receptor GID1, thus recruiting DELLAs for polyubiquitination by the the F-box protein gibberellin-insensitive dwarf2 (GID2), and the Skp, Cullin, F-box containing (SCF) ubiquitin ligase complex (SCF^{GID2}) and subsequent destruction in the 26S proteasome, thus promoting plant growth (*9,10,16,31-34*). We next found that reduced GID1 function in a NJ6-*gid1-10* mutant (*gid1* loss-of-function mutant; fig. S8B) increases tiller number above that of NJ6 controls in both high and low nitrogen supply (similar to NJ6-*sd1*; Fig. 3A, B). Conversely, transgenic NJ6-*sd1* plants overexpressing *GID1* under the control of the cauliflower mosaic virus (CaMV) 35S promoter exhibit nitrogen-insensitive responses, with lower tiller number than non-transgenic controls (Fig. 3B). Whilst gibberellin represses tiller number in both NJ6 and NJ6-*sd1*, it has no effect on tiller number in NJ6-*gid1-10*, NJ6-*sd1-ngr5* or in NJ6-*sd1* plants overexpressing *GID1* (Fig. 3B). Furthermore, either gibberellin-induced inhibition or GID1-mediated repression of tillering mimics the effect of *ngr5* (Fig. 3B). These results suggest that gibberellin-GID1 mediated repression of tiller number is dependent upon the nitrogen-regulated function of NGR5.

We next found that NGR5 abundance is negatively associated with gibberellin level: whilst NGR5-HA accumulation is increased in relatively gibberellin-deficient NJ6-*sd1* plants (versus NJ6), it is reduced by exogenous gibberellin treatment (Fig. 3C). Conversely, gibberellin-mediated decrease in NGR5-HA abundance is inhibited by treatment with the proteasome inhibitor MG132 (carbobenzoxy-Leu-Leu-leucinal), such that NGR5-HA accumulation is increased above that of NJ6-*sd1* plants (Fig. 3C). Accordingly, western blot analysis detected the accumulation of polyubiquitinated NGR5-HA in the presence of MG132 (Fig. 3D), suggesting that gibberellin promotes polyubiquitination and subsequent proteolysis of NGR5 in the 26S proteasome. In addition, gibberellin-induced degradation of NGR5-HA is inhibited in the NJ6-*gid1-10* mutant (Fig. 3E), indicating that gibberellin-induced promotion of NGR5 polyubiquitination and proteasome destruction is dependent upon the *GID1* function.

Gibberellin responses are conventionally considered to be activated by GID1-mediated destruction of DELLAs (*9*,*10*). However, we found that gibberellin-mediated degradation of NGR5-HA occurs either in the absence of DELLAs, in a loss-of-function *slr1* mutant (Fig. 3E; *11*), or in the presence of the high-level DELLA accumulation conferred by the *Slr1-d6* gain-of-function mutation (Fig. 3F; *35*). Whilst the mutant SLR1 DELLA encoded by *Slr1-d6* is relatively resistant to gibberellin-mediated destruction, NGR5-HA is still destabilized by

exogenous gibberellin treatment (Fig. 3F). Thus, although GID1-dependent, gibberellin promoted destabilization of NGR5 is neither dependent upon nor downstream of gibberellin-induced DELLAs destruction. We therefore explored the possibility of an alternative previously unknown DELLA-independent mechanism whereby the SCF^{GID2} E3 ubiquitin ligase directly mediates gibberellin-promoted destruction of NGR5. First, we found that GID1 interacts directly with NGR5 (as assayed by both split firefly luciferase complementation (SFLC) and Co-IP; Fig. 3G, H), and that the strength of this interaction is potentiated by increasing concentrations of gibberellin (Fig. 3H, I). Thus, as with the DELLAs, gibberellin enhances the interaction between NGR5 and GID1, identifying NGR5 as a potential alternative substrate for GID1-promoted polyubiquitination. Although NGR5 lacks the specific DELLA motif that enables the GID1-DELLA interaction (*33*,*34*), we found a motif within the AP2-R2 (repeated units 2; *18*) domain of NGR5 to enable the GID1-NGR5 interaction (fig. S10). Furthermore, NGR5 also interacts with the GID2 F-box component of the SCF^{GID2} E3 ubiquitin ligase that normally targets SLR1 for destruction in the 26S proteasome (Fig. 3J, K). Accordingly, an *in vitro* ubiquitination assay showed that GST (glutathione S-transferase)-NGR5 fusion protein is polyubiquitinated by GID2-Flag (ASP-TYR-LYS-ASP-ASP-ASP-ASP-LYS peptide) fusion protein in the presence of ubiquitin-activating enzyme E1, ubiquitin-conjugating enzyme E2 and ubiquitin, but not in the absence of GID2-Flag (Fig. 3L), suggesting that NGR5 is a substrate of the SCF^{GID2} E3 ubiquitin ligase. Additional time-course experiments showed that gibberellin promotes the progressive degradation of GST-NGR5, but that this degradation is inhibited both by MG132 and in *gid1-c1*, a CRISPR/Cas9-generated *GID1* loss-of-function mutant (Fig. 3M; fig. S8B). Finally, lack of GID2 function (in a *gid2-c1* mutant; fig. S8C) also inhibits gibberellin-mediated degradation of GST-NGR5 (Fig. 3M). We conclude that the gibberellin-mediated regulation of NGR5 is not due to gibberellin-promoted destruction of DELLAs, but is due to a previously unknown direct and gibberellin-potentiated interaction of NGR5-GID1, leading to polyubiquitination of NGR5 by the SCF^{GID2} E3 ubiquitin ligase and subsequent destruction in the proteasome.

DELLA-NGR5 modulation of tiller N-response

We next found that NGR5 interacts directly with SLR1 (in yeast two-hybrid screens; table S2; and in BiFC and Co-IP assays; fig. S11A, B). Nevertheless, we additionally found that the LC2-NGR5 interaction is not inhibited by the presence of SLR1 (fig. S12), suggesting that the SLR1-NGR5 interaction does not directly interfere with the LC2-NGR5 interaction that determines NGR5 function. Further experiments showed that the LHR1 (leucine heptad repeat

1) motif of the DELLA protein is necessary for the NGR5-SLR1 interaction (fig. S11C). Thus, in addition to both being substrates of gibberellin-GID1-SCF^{GID2}, SLR1 and NGR5 interact directly with one another. With the LHR1 motif being conserved in all the GRAS (derived from three initially identified members, GAI (gibberellin-insensitive), RGA (repressor of ga1-3), and SCARECROW) proteins, and we next found that NGR5 interacts with two additional GRAS proteins (DWARF AND LOW-TILLERING (DLT) and MONOCULM1 (MOC1)) previously shown to regulate tiller number (*17,19,36*; fig. S13A). The competitive nature of the SLR1-NGR5 relationship with respect to GID1 (fig. S13B; and hence with respect to GID1-promoted destruction) causes accumulation of NGR5-HA (conferred by *p35S::NGR5-HA*) to further increase the accumulation of SLR1 in 9311 (fig. S13C).

We next determined if competitive SLR1-NGR5-GID1 relationships also condition gibberellin and nitrogen effects on tiller number. As shown in Fig. 1B, the enhanced DELLA function conferred by the *Rht-B1b* allele results in increased tiller number. We therefore tested the possibility that the effect of *Rht-B1b* on tiller number might be due to differential effects on NGR5 stability. Accordingly, we found using FRET (Förster resonance energy transfer) analysis that the extent of the interaction between GID1 and NGR5 is reduced by the presence of Rht-B1b (Fig. 4A, B). We then confirmed the expectation that a reduced GID1-NGR5 interaction in the presence of Rht-B1b reduces the rate of proteasome-dependent GST-NGR5 destruction (Fig. 4C), and found similar reductions to be conferred by accumulation of wild-type Rht-B1a or SLR1 proteins (Fig. 4A-C). Further comparative studies showed His-NGR5 (His-tagged fusion protein) destruction to be more rapid than that of His-SLR1 (His-tagged fusion protein; Fig. 4D). Thus, although gibberellin-promoted NGR5 destruction is DELLA-independent (Fig. 3E, F), competition between NGR5 and SLR1 for GID1 interaction reduces the extent of NGR5-GID1 interaction (fig. S13B). Moreover, abundance of NGR5-GFP (green fluorescent protein) fusion protein (conferred by *p35S::NGR5-GFP*) is increased with PAC treatment, but reduced in response to combined gibberellin and PAC treatments (fig. S13D, E). This is also consistent with the observations that *ngr5* exhibits a higher ratio of gibberellin-induced leaf sheath growth, whereas transgenic plant overexpressing *NGR5-HA* displays reduced sensitivity to PAC treatment when compared with wild-type controls (fig. S14). We conclude that the enhanced DELLA function characteristic of both wheat and rice green revolution varieties competitively inhibits the GID1-NGR5 interaction, thus stabilizing NGR5 by reducing gibberellin-GID1 mediated destruction.

To determine if DELLA promotion of rice tillering is NGR5-dependent, 9311 NILs (near isogenic lines) carrying various combinations of different *SD1*, *GID1* and *NGR5* alleles were generated. Whilst the increased SLR1 accumulations in both 9311-*NGR5*-*gid1-10* and 9311-*NGR5*-*sd1* increase the tiller numbers of plants grown in either low or high nitrogen supply (versus 9311-*NGR5*-*SD1*), there is almost no difference in tiller number when 9311-*ngr5*-*sd1*, 9311-*ngr5*-*SD1* and 9311-*ngr5*-*gid1-10* are compared (Fig. 4E). Thus, the DELLA-mediated enhancement of nitrogen-induced tiller number increase typical of green revolution rice varieties is dependent upon NGR5 function. Accordingly, comparisons of NGR5-regulated mRNA abundance and H3K27me3 modification of branching inhibitory *D14* (Fig. 4F) and *OsSPL14* (Fig. 4G) genes in 9311 (containing *sd1*) versus 9311-*SD1* revealed mRNA abundance and modification status at 0.6N in 9311-*SD1* to be roughly equivalent to that at 0.2N in 9311-*sd1*. Thus, the enhanced DELLA function of *sd1* increases tiller number in response to nitrogen supply by increasing the stability of NGR5 (Fig. 3C, E), which in turn inhibits the expression of shoot branching inhibitor genes, thereby promoting tiller number.

NGR5 improves yield and nitrogen use-efficiency

We next determined if increase in NGR5 abundance beyond that seen in elite rice varieties (e.g., *sd1*-containing 9311) could further increase tiller number and yield in reduced nitrogen fertilizer inputs. First, we surveyed publicly available rice varietal genome sequence data for natural genetic variation at *NGR5* (*37*), distinguishing five distinct haplotypes (Hap.1-Hap.5; Fig. 4H), and finding that Hap.2 is associated with increased *NGR5* mRNA abundances in both low and high nitrogen conditions (fig. S15), together with increases in tiller number and field-grown grain yield of 686 diverse Asian cultivated rice accessions (Fig. 4I). Further analysis showed that Hap.2-containing Guichao2 (Guichao2 (Hap.2), one of the highest yielding of *indica* varieties cultivated in China since the 1980s) displayed a greater *NGR5* mRNA abundance than Guichao2 (Hap.1) (a NIL carrying Hap.1 in the Guichao2 genetic background) and other lines (including Hap.5-containing 9311), even at low and moderate nitrogen supply (Fig. 4J). In addition, we showed that a transgenic mimic of Hap.2 (expression from a *p35S::NGR5* transgene) enhanced 9311 grain yield in a range of nitrogen supply conditions, without affecting the characteristic and beneficial semi-dwarfism of 9311 (Fig. 4K, L), thus suggesting that breeding with Hap.2 is a feasible future strategy towards improving nitrogen use-efficiency of the elite rice varieties. Finally, having recently shown that allelic variation at *GRF4* (encoding the rice GROWTH-REGULATING FACTOR 4 transcription factor) enhances grain yield and nitrogen use-efficiency through coordinating effects on carbon and

nitrogen metabolic regulation (*13*), we investigated the genetic interaction between *GFR4* and *NGR5*, finding that combined increased abundances of both *GRF4* and *NGR5* further enhances 9311 yield and nitrogen use-efficiency, particularly at relatively low levels of nitrogen supply (Fig. 4M).

In summary, we have shown that nitrogen determines genome-wide chromatin status (specific H3K27me3 histone modification) via NGR5-dependent recruitment of the polycomb complex PRC2 to target genes, amongst which are tiller-branch repressing genes. In consequence, repression of tiller outgrowth is reduced in increasing nitrogen supply, causing increased tillering. We have also shown that NGR5 is a non-DELLA target of gibberellin-GID1-SCF^{GID2} mediated proteasomal destruction, and that competitive NGR5-DELLA-GID1 interactions cause the NGR5-dependent yield-enhancing tillering increases typical of green revolution rice varieties. Because NGR5 is already known to be involved in the cross-talk between auxin and brassinosteroid signaling (*19*,*20*), our discoveries add to a growing understanding of how diverse modes of molecular and functional cross-talk between multiple phytohormonal signaling and fertilizer use responses function in the environmentally adaptive regulation of plant growth and development. Finally, we have shown that increasing NGR5 expression or activity provides a breeding strategy to reduce nitrogen fertilizer use whilst boosting grain yield above what is currently sustainably achievable.

Materials and Methods

Plant materials and growth conditions

A nitrogen-insensitive rice mutant, designated *ngr5* (*nitrogen-mediated tiller growth response 5*), was isolated from the progeny of EMS-mutagenized *indica* cultivar 9311. Near-isogenic lines (NILs) carrying allelic combinations of the *NGR5*, *SD1* and *GID1* loci were obtained by backcrossing to recurrent parent 9311 (or NJ6) six times. Details of the germplasm used for the positional cloning and haplotype analysis have been described elsewhere (*13*,*37*-*39*). Paddy-grown rice plants, including 686 diverse Asian cultivated rice accessions (*37*), were planted in rows 20 cm apart and raised in standard paddy conditions at two experimental stations, one in Lingshui (Hainan Province), the other in Hefei (Anhui Province).

Hydroponic culture conditions

Hydroponic culture conditions have been described elsewhere (*13*). Rice seeds were surface sterilized with 20% sodium hypochlorite solution for 30 min, then rinsed and soaked in water for 3 days to allow the seeds to germinate. Surface-sterilized seeds were then germinated in moist Perlite. 7-day-old seedlings were transplanted to PVC pots containing 40 L nutrient solution (1.25 mM NH_4NO_3, 0.5 mM $NaH_2PO_4 \cdot 2H_2O$, 0.75 mM K_2SO_4, 1 mM $CaCl_2$, 1.667 mM $MgSO_4 \cdot 7H_2O$, 40 μM Fe-EDTA (Na), 19 μM H_3BO_3, 9.1 μM $MnSO4 \cdot H_2O$, 0.15 μM $ZnSO_4 \cdot 7H_2O$, 0.16 μM $CuSO_4$, and 0.52 μM $(NH_4)_3Mo_7O_{24} \cdot 4H_2O$, pH 5.5), and growth was continued in a greenhouse. Compositions of nutrient solutions containing different levels of supplied nitrogen were as follows: 1N, 1.25 mM NH_4NO_3; 0.6N, 0.75 mM NH_4NO_3; 0.2N, 0.25 mM NH_4NO_3; 0N, 0 mM NH_4NO_3. All nutrient solutions were changed twice per week, pH was adjusted to 5.5 every day. The temperature was maintained at 30 °C day and 22 °C night, and the relative humidity was 70%.

Map-based cloning of *NGR5*

Fine-scale mapping of *ngr5* was based on 600 F_2 plants and 1,256 BC_1F_2 plants derived from a cross between the *ngr5* mutant and the *japonica* rice cultivar Lansheng (recurrent parent). Genomic DNA sequences in the candidate region were compared between 9311, Nipponbare and Lansheng. Primer sequences used for map-based cloning and genotyping assays are given in table S7.

Transgene constructs

Wild-type *NGR5* and *ngr5* mRNA-encoding sequences (together with intron sequences and/or promoter regions lying 3-kbp upstream of the transcription start site) were amplified from 9311 and *ngr5* mutant plants, respectively. These amplified genomic DNA fragments were inserted into the *p35S::HA-nos* (*40*) and *pCAMBIA1300* (CAMBIA, www.cambia.org) vectors to respectively generate *pNGR5::NGR5*, *pNGR5::ngr5*, *pNGR5::NGR5-HA* and *p35S::NGR5* constructs. Full-length cDNAs of *NGR5*, *GID1* and *LC2* cDNAs were amplified from 9311 plants, and inserted into *p35S::HA-nos* (*40*) or *p35::GFP-nos* (*39-41*) vector to respectively generate *p35S::GID1*, *p35S::LC2-HA*, *p35S::NGR5-HA* and *p35S::NGR5-GFP* constructs. gRNA constructs required for CRISPR/Cas9-mediated generation of *GID1*, *GID2* and *LC2* mutant alleles were made as described elsewhere (*13*,*41*). The transgenic rice plants were generated by *Agrobacterium*-mediated transformation as described elsewhere (*42*). Relevant primer sequences are given in table S8.

qRT-PCR analysis

Total RNAs were extracted from tiller buds of 3-week-old rice plants using the TRIzol reagent (Invitrogen) according to the manufacturer's protocol, and treated with RNase-free DNase I (Invitrogen) to remove contaminating genomic DNAs. The full-length cDNAs were then reverse-transcribed using a cDNA synthesis kit (TRANSGEN, AE311-02). Subsequent qRT-PCR processing steps were performed according to the manufacturer's instructions (TRANSGEN, AQ101), with each qRT-PCR assay being replicated at least three time with three independent RNA preparations. Rice *Actin1* gene (*OsActin1*, LOC_Os03g50885) transcripts were used as an internal reference. Relevant primer sequences are given in table S9.

Yeast two-hybrid assays

Yeast two-hybrid screening was performed as described elsewhere (*38*). The full length *NGR5* cDNA was amplified and subcloned into *pGBKT7* (Takara Bio Inc.), then transformed into yeast strain AH109. The NGR5 protein was used as a bait to screen a cDNA library prepared from equal amounts of poly(A)-containing RNA sampled from various rice tissues/organs, including tiller buds, roots, leaves, shoot apical meristem (SAM) and young panicles etc. Experimental procedures for screening and plasmid isolation were performed according to the manufacturer's user guide. cDNAs encoding various deleted and non-deleted versions of SLR1 were amplified and then subcloned into the *pGBKT7* vector (Takara Bio Inc.). Bait and prey vectors were co-transformed into yeast strain AH109, and experimental procedures were performed according to the manufacturer's instructions (Takara Bio Inc.). Relevant primer sequences are given in table S8.

Bimolecular fluorescence complementation (BiFC) assays

As described previously (*13*), full-length cDNAs of *NGR5*, *LC2* and *SLR1*, *DLT* and *MOC1* were amplified from 9311, and inserted into *pSY-735-35S-cYFP-HA* or *pSY-736-35S-nYFP-EE* vectors to generate fusion constructs. Co-transfection of constructs (e.g., nYFP-NGR5 and cYFP-LC2) into tobacco leaf epidermal cells by *Agrobacterium*-mediated infiltration enabled testing for protein-protein interaction. Following 48 hours incubation in the dark, the YFP signal was captured using a confocal microscope (Zeiss LSM710). Each BiFC assay was repeated at least three times. Relevant primer sequences are given in table S8.

Split firefly luciferase complementation (SFLC) assays

Full-length cDNAs of *GID1* and *GID2,* and cDNAs encoding various deleted and non-deleted versions of *NGR5* were amplified from 9311, and then inserted into *pCAMBIA1300-35S-Cluc-RBS* or *pCAMBIA1300-35S-HA-Nluc-RBS* vectors (*39*) to generate fusion constructs. Two different vectors (e.g., nLUC-GID1 and cLUC-NGR5) enabling testing of protein-protein interaction, together with the p19 silencing plasmid, were co-transfected into tobacco leaf epidermal cells by *Agrobacterium*-mediated infiltration. Following 48 hours incubation in the dark, the injected leaves were sprayed with 1 mM luciferin (Promega, E1605) and the LUC signal was captured using a cooled CCD imaging apparatus (Berthold, LB985). Each assay was repeated at least three times. Relevant primer sequences are given in table S8.

FRET (Förster resonance energy transfer) assays

FRET assays were performed as previously described (*13*). Cauliflower mosaic virus (CaMV) 35S promoter-driven fusion constructs with C-terminal tagging CFP or YFP were created to generate the donor vectors *p35S::GID1-CFP* (or *p35S::LC2-CFP*), and the acceptor vector *p35S::NGR5-YFP*. Donor and acceptor vectors, with or without *p35S::Rht-B1a* (*p35S::Rht-B1b*, or *p35S::SLR1*) vector, were co-transformed into tobacco leaf epidermis cells by *Agrobacterium*-mediated vacuum infiltration to provide the FRET measurements. Transformation with the *p35S::GID1-CFP* vector only provided the donor channel, and with the *p35S::NGR5-YFP* vector only the acceptor channel. The FRET signal was detected and photographed using a confocal microscope (Zeiss LSM710). Relevant primer sequences are given in table S8.

Western blotting and co-immunoprecipitation (Co-IP) assays

Protein extracts were electrophoretically separated by SDS-PAGE and transferred to a nitrocellulose membrane (GE Healthcare). Proteins were detected by immunoblot using the following antibodies: anti-SLR1 (ABclonal Technology), anti-HA (MBL, M180-7), anti-Ubiquitin (Abcam, ab134953), anti-GST (Santa Cruz, sc-138), anti-GFP (Abcam, ab6673), and anti-HSP90 (BGI), respectively. For Co-IP experiments, full-length *NGR5*, *LC2*, *SLR1*, *GID1* and *GID2* cDNAs were amplified, then inserted into either the *pUC-35S-HA-RBS* or the *pUC-35S-Flag-RBS* vector as previously described (*13*,*39*). Rice protoplasts were transfected with 100 μg of plasmid DNA and then incubated overnight in the dark. Total protein was extracted from harvested protoplasts with a lysis buffer (50 mM HEPES (pH7.5), 150 mM KCl, 1 mM EDTA, 0.5% Trition-X 100, 1 mM DTT, proteinase inhibitor cocktail (Roche LifeScience)). Lysates were incubated with magnetic beads conjugated with an anti-DDDDK-tag antibody

(MBL, M185-11) or anti-HA-tag antibody (MBL, M180-11) at 4 °C for 4 hours. The magnetic beads were then washed 5 times with TBS-T buffer (500 mM NaCl, 20 mM Tris-HCl (pH8.0), 0.1% Tween 20) and eluted with 3×Flag peptide (Sigma-Aldrich, F4709). Immunoprecipitates were electrophoretically separated and specific proteins detected by immunoblotting with anti-HA (MBL, M180-7) or anti-DDDDK (MBL, M185-7) antibodies. Relevant primer sequences are given in table S8.

***In vivo* pull-down**

A full-length rice *GID1* cDNA was amplified and then inserted into the *pGEX-4T-1* vector (GE Healthcare). The recombinant GST-GID1 protein was expressed in *Escherichia coli* BL21 (DE3) (Transgen, CD701-01), and then purified and immobilized on Glutathione Sepharose 4B beads (GE Healthcare, 17-0756) following the manufacturer's instructions. The beads were divided into four equal aliquots, and incubated with the same amount of NGR5-HA (or NGR5-Flag) protein lysate, together with His-SLR1 or with different concentrations of GA_3 (0, 2, 5, 10 μM) and/or MG132 (50 μM) for 2 hours at 4 °C. The beads were subsequently washed five times with TBS-T buffer, followed by elution with 50 μL elution buffer (50 mM Tris-HCl, 10 mM reduced glutathione, pH 8.0). Supernatants were resolved by 12% SDS-PAGE and subjected to immunoblotting using anti-GST (Santa Cruz, sc-138) and anti-HA (MBL, M180-7) antibodies. Relevant primer sequences are given in table S8.

EMSA assays

EMSA assays were performed as previously described (*39*). A full-length *NGR5* cDNA was amplified and inserted into the *pGEX-4T-1* vector (GE Healthcare). Recombinant GST-NGR5 protein was expressed in *E. coli* BL21 (DE3) strain and purified using Glutathione Sepharose 4B (GE Healthcare, 17-0756) following the manufacturer's instructions. DNA probes (D5 fragment for the *D14* gene, S3 fragment for the *OsSPL14* gene) were amplified and labelled using a biotin label kit (Biosune). DNA gel shift assays were performed using the LightShift Chemiluminescent EMSA kit (Thermo Fisher Scientific, 20148). Relevant primer sequences are given in table S10.

Cell-free protein degradation assays

3-week-old NJ6-*gid1-c1* and NJ6-*gid2-c1* seedlings (together with NJ6) were harvested and ground into a fine powder in liquid nitrogen. Lysates were subsequently extracted with lysis buffer (25 mM Tris-HCl (pH 7.5), 10 mM NaCl, 10 mM $MgCl_2$, 4 mM PMSF, 5 mM DTT and

10 mM ATP) as described elsewhere (*43*), total protein extracts were adjusted to be at equal concentration in the lysis buffer for each assay. 200 μL of rice cell lysates were incubated with 100 ng of purified GST-NGR5 (or His-NGR5) fusion protein in the presence or absence of the recombinant Rht-B1b-Flag, Rht-B1a-Flag, SLR1-Flag or His-SLR1 proteins. Proteins were extracted from lysates that had either been exposed or not to treatments with 100 μM GA_3 and/or 100 μM MG132 for a series of incubation times and then subjected to SDS-PAGE and western blotting using an anti-GST antibody (Santa Cruz, sc-138). HSP90 was employed as a loading control.

***In vitro* protein ubiquitination assays**

Full-length *GID2* cDNA was amplified and inserted into *PUC-35S-flag-RBS* vector (*39*). Rice protoplasts were transfected with 100 μg of plasmid and incubated for 24 hours. Total protein was extracted from harvested protoplasts in the lysis buffer (50 mM HEPES (pH7.5), 150 mM KCl, 1 mM EDTA, 0.5% Trition-X 100, 1 mM DTT and proteinase inhibitor cocktail (Roche LifeScience)). Lysates were incubated with agarose-conjugated anti-Flag antibodies (Sigma-Aldrich, A2220) at 4°C for 2 hours, rinsed 6 times in the PBS-T buffer, and then eluted with 3×Flag peptide (Sigma-Aldrich). Purified GID2-Flag proteins were used for *in vitro* ubiquitination assays as previously described (*44*). Crude extracts containing recombinant GST-NGR5, purified E3 (GID2-Flag), 6×His-tagged Ubiquitin (Ub), E1 and E2 (Ubiquitinylation kit; Enzo Life Science, BML-UW9920-0001) were used. Buffer at a final concentration of 50 mM Tris-HCl (pH 7.4), 5 mM $MgCl_2$, and 2 mM ATP was also added to the system. The reactions were incubated at 30°C for 2 hours, and terminated by adding SDS sample buffer with β-Mercaptoethanol. Reaction products were separated with 12% SDS-PAGE and subjected to immunoblotting using anti-ubiquitin antibody (Abcam, ab134953) and anti-GST antibody (Santa Cruz, sc-138). Relevant primer sequences are given in table S8.

ChIP-PCR assay

ChIP assays were performed as described elsewhere (*13*). 2 g of 2-week-old rice plants were collected and immediately fixed with 1% (v/v) formaldehyde under vacuum for 15 min at 25°C, and then homogenized in liquid nitrogen. After the nuclei were isolated and lysed, the chromatin was ultrasonically fragmented on ice to an average size of 500 bp. Immunoprecipitations were performed with an anti-HA antibody (Santa Cruz, sc-7932x) and an anti-H3K27me3 antibody (Millipore, 07-449) overnight at 4 °C. At the same time, an equal volume of the supernatant was prepared without any antibody as a mock sample. The bound

DNA fragments were then reversely released and amplified by real-time quantative PCR. Relevant primer sequences are listed in table S11.

RNA-seq

Total RNAs were extracted from tiller buds of 3-week-old 9311 plants treated with and without gibberellin and *ngr5* mutants grown in high N (1.25 mM NH_4NO_3) supply conditions using the TRIzol reagent (Invitrogen) according to the manufacturer's instructions. Libraries were constructed and sequenced using the BGISEQ-500 sequencer. Raw sequencing reads were cleaned by removing adaptor sequences, reads containing poly-N sequences, and low-quality reads, and clean reads were then mapped to the Nipponbare reference genome as described elsewhere (*13*).

ChIP-seq

ChIP-Seq analysis was performed as previously described (*13*). Approximately 2 g of 2-week-old transgenic plants carrying the *p35S::LC2-HA* and *pNGR5::NGR5-HA* constructs grown in high N (1N, 1.25 mM NH_4NO_3) supply conditions, and of *ngr5* and wild-type plants grown in low (0.2N, 0.25 mM NH_4NO_3) or high nitrogen (1N, 1.25 mM NH_4NO_3) supply conditions with or without 100 μM GA_3 (Sigma-Aldrich, G1025) and 10 μM PAC (Sigma-Aldrich, 19847) treatments, were fixed with 1% (v/v) formaldehyde under vacuum for 15 min at 25°C, and then homogenized in liquid nitrogen. Following cell lysis and nucleic acid isolation, cross-linked chromatin fibers were ultrasonically fragmented into fragments of an average size of 500 bp. Immunoprecipitations were performed with anti-HA antibodies (Santa Cruz, sc-7932) and anti-H3K27me3 antibodies (Millipore, 07-449) overnight at 4 °C. The precipitated DNA was recovered by centrifugation (13,000 x g, 5 min, 25 °C) and dissolved in sterile distilled water. Illumina sequencing libraries were constructed according to the manufacturer's instructions, and then sequenced on the BGISEQ-500 platform. Sequencing reads were mapped to the reference genome as previously described (*13*). The precipitated DNA samples served also as template for quantitative real-time PCR. Relevant primer sequences are given in table S11.

Processing of ChIP- and RNA-sequencing data

Sequencing reads were cleaned with Trimmomatic (version 0.36; *45*) and Sickle, including elimination of bases with low-quality scores (< 25) and irregular GC contents, as well as removal of sequencing adapters and short reads. The remaining clean reads were mapped to the genome of japonica rice (MSU7.0 release) with the Burrows-Wheeler Aligner-backtrack

(version 0.7.16a-r1181; *46*) for ChIP-sequencing data and HISAT2 2.1.0 (*47*) for RNA-seq data. MACS (version 1.3.7; *48*) was used to identify read-enriched regions (peaks) of ChIP-sequencing data based on the following combined criteria: *P* value < 1e−5 and fold-change > 32. Target genes were defined as genes with a peak within or near the gene body (± 2 kb). DESeq (*49*) was applied to determine the significance of the differential expression between samples with the combined criteria: fold change > 2 and adj. $P < 0.05$.

Gene set enrichment analysis

To determine the enrichment of H3K27me3 targets in *NGR5* regulated genes, i.e. differentially expressed genes in ngr5, gene set enrichment analysis (GSEA) was performed, which is a robust computational method that determines whether an *a priori* gene set shows statistically significant and concordant differences between two samples (*50*). Briefly, *NGR5* regulated genes were ranked by the quantitative expression change in *ngr5*, followed by calculation of the fraction of regulated genes that are targeted by H3K27me3. The enrichment score is normalized by the size of the gene set (NES). *P* value is estimated by permutating genes.

Statistical analysis

Data were statistically analysed and multiple comparisons were made using Duncan's multiple range test as described elsewhere (*13*). *P*-values of less than 0.05 were considered to indicate statistical significance. Statistical calculations were performed using Microsoft Excel 2010.

REFERENCES AND NOTES

1, G.S. Khush, Green revolution: preparing for the 21st century. *Genome* **42**, 646-655 (1999).

2, P.L. Pingali, Green Revolution: Impacts, limits, and the path ahead. *Proc. Natl. Acad. Sci. USA* **109**, 12302-12308 (2012).

3, R. E. Evenson, D. Gollin, Assessing the impact of the green revolution, 1960 to 2000. *Science* **300**, 758-762 (2003).

4, P. Hedden, The genes of the Green Revolution. *Trends Genet.* **19**, 5-9 (2003).

5, J. Peng, *et al*., Green revolution genes encode mutant gibberellin response modulators. *Nature* **400**, 256-261 (1999).

6, C. Zhang, L. Gao, J. Sun, J. Jia, Z. Ren, Haplotype variation of Green Revolution gene *Rht-D1* during wheat domestication and improvement. *J. Integr. Plant Biol.* **56**, 774-780 (2014).

7, A. Sasaki, *et al*., Green revolution: a mutant gibberellin-synthesis gene in rice. *Nature* **416**, 701-702 (2002).

8, W. Speilmeyer, M. H. Ellis, P. M. Chandler, Semidwarf (*sd-1*), "green revolution" rice, contains a defective gibberellin 20-oxidase gene. *Proc. Natl. Acad. Sci. USA* **99**, 9043-9048 (2002).

9, N. P. Harberd, E. Belfield, Y. Yasumura, The angiosperm gibberellin-GID1-DELLA growth regulatory mechanism: how an "inhibitor of an inhibitor" enables flexible response to fluctuating environments. *Plant Cell* **21**, 1328-1339 (2009).

10, H. Xu, Q. Liu, T. Yao, X. Fu, Shedding light on integrative GA signaling. *Curr. Opin. Plant Biol.* **21**, 89-95 (2014).

11, H. Itoh, M. Ueguchi-Tanaka, Y. Sato, M. Ashikari, M. Matsuoka, The gibberellin signaling pathway is regulated by the appearance and disappearance of SLENDER RICE1 in nuclei. *Plant Cell* **14**, 57-70 (2002).

12, K. Asano, *et al*., Artificial selection for a green revolution gene during *japonica* rice domestication. *Proc Natl. Acad. Sci. USA.* **108**, 11034-11039 (2011).

13, S. Li, *et al*., Modulating plant growth-metabolism coordination for sustainable agriculture. *Nature* **560**, 595-600 (2018).

14, H. Sun, *et al*., Heterotrimeric G proteins regulate nitrogen-use efficiency in rice. *Nat Genet.* **46**, 652-656 (2014).

15, G. W Wu, L. T. Wilson, A. M. McClung, Contribution of rice tillers to dry matter accumulation and yield. *Agron J.* **90**, 317-323 (1962).

16, M. Ueguchi-Tanaka, *et al*., GIBBERELLIN INSENSITIVE DWARF1 encodes a soluble receptor for gibberellin. *Nature* **437**, 693-698 (2005).

17, Z. Liao, *et al*., SLR1 inhibits MOC1 degradation to coordinate tiller number and plant height in rice. *Nat Commun.* **10** 2738 (2019).

18, K. Aya, *et al*., A novel AP2-type transcription factor, SMALL ORGAN SIZE1, controls organ size downstream of an auxin signaling pathway. *Plant Cell Physiol.* **55**, 897-912 (2014).

19, K. Hirano, *et al*., SMALL ORGAN SIZE 1 and SMALL ORGAN SIZE 2/DWARF AND LOW-TILLERING form a complex to integrate auxin and brassinosteroid signaling in rice. *Mol Plant* **10**, 590-604 (2017).

20, S. Qiao, *et al*., The RLA1/SMOS1 transcription factor functions with OsBZR1 to regulate brassinosteroid signaling and rice architecture. *Plant Cell* **29**, 292-309 (2017).

21, R. Yao, *et al*., DWARF14 is a non-canonical hormone receptor for strigolactone. *Nature* **536**, 469-473 (2016).

22, L. Jiang, *et al*., DWARF 53 acts as a repressor of strigolactone signalling in rice. *Nature* **504**, 401-405 (2013).

23, F. Zhou, *et al*., D14-SCF(D3)-dependent degradation of D53 regulates strigolactone signalling. *Nature* **504**, 406-410 (2013).

24, S. Ishikawa, *et al*., Suppression of tiller bud activity in tillering dwarf mutants of rice. *Plant Cell Physiol.* **46**, 79-86 (2005).

25, T. Takeda, *et al.*, The OsTB1 gene negatively regulates lateral branching in rice. *Plant J* **33**, 513-520 (2003).

26, Y. Jiao, *et al*., Regulation of OsSPL14 by OsmiR156 defines ideal plant architecture in rice. *Nat Genet.* **42**, 541-544 (2010).

27, K. Miura, *et al*., OsSPL14 promotes panicle branching and higher grain productivity in rice. *Nat Genet.* **42**, 545-549 (2010).

28, S. Wang, *et al*., Non-canonical regulation of SPL transcription factors by a human OTUB1-like deubiquitinase defines a new plant type rice associated with higher grain yield. *Cell Res.* **27**, 1142-1156 (2017).

29, T. Arite, *et al*., d14, a strigolactone-insensitive mutant of rice, shows an accelerated outgrowth of tillers. *Plant Cell Physiol.* **50**, 1416-1424 (2009).

30, J. Wang, J. Hu, Q. Qian, H. W. Xue, LC2 and OsVIL2 promote rice flowering by photoperoid-induced epigenetic silencing of *OsLF*. *Mol Plant* **6**, 514-527 (2013).

31, A. Sasaki, *et al*., Accumulation of phosphorylated repressor for gibberellin signaling in an F-box mutant. *Science* **299**, 1896-1898 (2003).

32, X. Fu, *et al*., The Arabidopsis mutant sleepy1gar2-1 protein promotes plant growth by increasing the affinity of the SCF^{SLY1} E3 ubiquitin ligase for DELLA protein substrates. *Plant Cell* **16**, 1406-1418 (2004).

33, K. Murase, Y. Hirano, T. P. Sun, T. Hakoshima, Gibberellin-induced DELLA recognition by the gibberellin receptor GID1. *Nature* **456**, 459-463 (2008).

34, A. Shimada, *et al*., Structural basis for gibberellin recognition by its receptor GID1. *Nature* **456**, 520-523 (2008).

35, Z. Wu, *et al*., Characterization of a new semi-dominant dwarf allele of SLR1 and its potential application in hybrid rice breeding. *J Exp Bot.* **69**, 4703-4713 (2018).

36, H. Tong, *et al*., DWARF AND LOW-TILLERING, a new member of the GRAS family, plays positive roles in brassinosteroid signaling in rice. *Plant J*. **58**, 803-816 (2009).

37, W. Wang, *et al*., Genomic variation in 3,010 diverse accessions of Asian cultivated rice. *Nature* **557**, 43-49 (2018).

38, S. Wang, *et al*., The *OsSPL16-GW7* regulatory module determines grain shape and simultaneously improves rice yield and grain quality. *Nat Genet.* **47**, 949-954 (2015).

39, Q. Liu, *et al*., G-protein βγ subunits determine grain size through interaction with MADS-domain transcription factors in rice. *Nat Commun.* **9**, 852 (2018).

40, S. Wang, *et al*., Control of grain size, shape and quality by OsSPL16 in rice. *Nat Genet.* **44**, 950-954 (2012).

41, X. Ma, *et al*., A robust CRISPR/Cas9 system for convenient, high-efficiency multiplex genome editing in monocot and dicot plants. *Mol Plant* **8**, 1274-1284 (2015).

42, X. Huang, *et al*., Natural variation at the *DEP1* locus enhances grain yield in rice. *Nat Genet.* **241**, 494-497 (2009).

43, F. Wang, *et al*., Biochemical insights on degradation of Arabidopsis DELLA proteins gained from a cell-free assay system. *Plant Cell* **21**, 2378–2390 (2009).

44, Q. Zhao, *et al*., A plant-specific in vitro ubiquitination analysis system. *Plant J.* **74**, 524-533 (2013).45, A. M. Bolger, M. Lohse, B. Usadel, Trimmomatic: a flexible trimmer for Illumina sequence data. *Bioinformatics* **30**, 2114-2120 (2014).

46, H. Li, R. Durbin, Fast and accurate short read alignment with Burrows-Wheeler transform. *Bioinformatics* **25**, 1754-1760 (2009).

47, D. Kim, B. Langmead, S. L. Salzberg, HISAT: a fast spliced aligner with low memory requirements. *Nature methods* **12**, 357-360 (2015).

48, Y. Zhang, *et al*., Model-based analysis of ChIP-Seq (MACS). *Genome biology* **9**, R137 (2008).

49, S. Anders, W. Huber, Differential expression analysis for sequence count data. *Genome biology* **11**, R106 (2010).

50, A. Subramanian, *et al*., Gene set enrichment analysis: a knowledge-based approach for interpreting genome-wide expression profiles. *Proc. Natl. Acad. Sci. USA* **102**, 15545-15550 (2005).

ACKNOWLEDGMENTS

We thank Prof. C. Sun for providing the CSSLs, Prof. Q. Qian for providing *d14*, Prof. Z. Cheng for providing *Slr1-d6*, and Prof. M. Matsuoka for the critical comments on the manuscript. **Funding:** This research work was supported by the National Key Research and Development Program of China (2016YFD0100401, 2016YFD0100706), the National Key

Program on Transgenic Research from the Ministry of Agriculture of China (2016ZX08009-001, 2016ZX08009-003), the National Natural Science Foundation of China (31830082, 31921005, 91935301, 31970304), the Strategic Priority Research Program of the Chinese Academy of Sciences (XDB27010000), and by the Biological and Biotechnological Sciences Research Council (UK) 'Newton Fund' Rice Research Initiative grant BB/N013611/1. **Author contributions:** K.W. performed most of the experiments; K.W., B.L. and Y.W. conducted the *NGR5* mutation screening; S.W. and K.W. performed map-based cloning and genetic complementation; K.W., W.S., J.C. and J.Z. constructed NILs and mutant plants; K.W., S.W., S.L. and Q.L. characterized the phenotypes of transgenic plants; W.S., X.W. and K.W. conducted protein-protein interactions; K.W., Y.Z. and J.W. performed field experiments; M.W., K.W. and Y.J.Z. performed analysis of ChIP-seq and RNA-seq; Y.W. and J.Y. performed haplotype analysis; K.W., N.P.H and X.F. designed experiments. N.P.H. and X.F. wrote the manuscript. All authors discussed and commented on the manuscript. **Competing interests:** The authors declare no competing interests. **Data and materials availability:** The raw sequence data reported in this paper have been deposited in the Genome Sequence Archive in BIG Data Center of CRA002108 that are publicly accessible at https://bigd.big.ac.cn/gsa. Requests for materials should be addressed to X.F. All of the data pertaining to the work are contained within the figures and supplementary materials.

SUPPLEMENTARY MATERIALS

Material and Methods

Figs. S1 to S15

Tables S1 to S11

References (*38-50*)

Figure Legends

Figure 1. NGR5 mediates nitrogen-dependent promotion of tillering. (**A**, **B**) Tiller numbers of field-grown rice and wheat plants in response to nitrogen supply. A, NJ6 versus NJ6-*sd1*. B, *Rht-B1a* versus *Rht-B1b*. Data shown as mean ± SE (n = 30) (**C**) Mature plants grown in low (90 kg/ha; LN) versus high (180 kg/ha; HN) nitrogen supply. Scale bar, 20 cm. (**D**) Tiller numbers at LN (90 kg/ha) versus HN (180 kg/ha). Data shown as mean ± SE (n = 20). (**E**)

NGR5 mRNA abundance in tiller buds. 3-week-old plants were grown hydroponically with varying nitrogen supply (0.2N, 0.25 mM NH_4NO_3; 0.6N, 0.75 mM NH_4NO_3; 1N, 1.25 mM NH_4NO_3), mRNA abundance relative to that of 0N (set to one). Data shown as mean ± SE (n = 3). (**F**) Accumulation of NGR5-HA in tiller buds of 3-week-old plants (as shown in **E**). Heat shock protein 90 (HSP90) serves as loading control. (**G**) Tiller numbers of field-grown rice plants under increasing nitrogen supply. Data shown as mean ± SE (n = 20). Different letters denote significant differences ($P < 0.05$; panels **A**, **B**, **D**, **E** and **G**; Duncan's multiple range test).

Figure 2. Nitrogen regulates tillering via H3K27me3 reprogramming. (**A**) BiFC assays. Scale bar, 60 μm. (**B**) Co-IP assays. (**C**) Mature plants grown in low (90 kg/ha; LN) versus high (180 kg/ha; HN) nitrogen supply. Scale bar, 20 cm. (**D**) Tiller number. Data shown as mean ± SE (n = 20). (**E**) Genome-wide surveys of H3K27me3 enrichment density. Each peak was normalized to zero mean and unit of energy (z-score). (**F**) Overlap of H3K27me3 ChIP-seq peaks. (**G**, **H**) Sequence motifs enriched during ChIP-seq with NGR5-HA (**G**) and LC2-HA (**H**). (**I**, **J**) Comparisons of mRNA abundance and H3K27me3 modification of *D14* (**I**) and *OsSPL14* (**J**) between 9311 and *lc2*. (**K**, **L**) Transcript abundance and H3K27me3 modification of *D14* (**K**) and *OsSPL14* (**L**) in 9311 with or without 100 μM GA_3 treatment. RT-PCR and ChIP experiments (**F, I-L**) were performed using tiller buds of 3-week-old plants grown in increasing nitrogen supply (0.2N, 0.25 mM NH_4NO_3; 0.6N, 0.75 mM NH_4NO_3; 1N, 1.25 mM NH_4NO_3). mRNA abundance relative to that of WT in 1N (set to one). Data (**I-L**) shown as mean ± SE (n = 3). Different letters denote significant differences ($P < 0.05$; panels **D** and **I-L**; Duncan's multiple range test).

Figure 3. Gibberellin-GID1-SCF^{GID2} targets NGR5 for destruction. (**A**) Mature plants grown in low (90 kg/ha; LN) versus high (180 kg/ha; HN) nitrogen supply. Scale bar, 20 cm. (**B**) Tiller number. Data shown as mean ± SE (n = 20). (**C**) Immunodetection of NGR5-HA. (**D**) Immunodetection of polyubiquitinated NGR5-HA. (**E**) Accumulation of NGR5-HA. (**F**) Effects of gibberellin on NGR5-HA and SLR1 accumulation. Total protein (**C**-**F**) was extracted from tiller buds of 3-week-old plants treated for 4 h with either 1 μM GA_3 and/or 100 μM MG132, HSP90 serves as loading control. (**G**) SFLC assays. (**H**) Co-IP assays. (**I**) Pull-down assays. (**J**) SFLC assays. Either nLUC-tagged GID1 (**G**) or nLUC-tagged GID2 (**J**) was co-transformed into tobacco leaves along with cLUC-targeted NGR5. (**K**) Co-IP assays. (**L**) *In vitro* ubiquitination assay. The immunoprecipitated GID2-Flag proteins transiently expressed

in rice protoplasts were used in an *in vitro* ubiquitination reaction in the presence of E1, E2 (UbcH5B), His-Ub and GST-NGR5. (**M**) Gibberellin-GID1-SCF^{GID2} destabilizes GST-NGR5. Lysates from NJ6, NJ6-*gid1-c1* and NJ6-*gid2-c1* plants were co-incubated with GST-NGR5 in the presence or absence of 100 μM GA_3 and 100 μM MG132. The lysates were harvested at various incubation times and immunoblotted to assess the accumulation of NGR5 and HSP90.

Figure 4. Balanced DELLA-NGR5 interactions improve nitrogen use-efficiency. (**A**) FRET images. Scale bar, 200 μm. (**B**) Mean N-FRET data for GID1-CFP and NGR5-YFP channels. Data shown as mean ± SE (n = 5) (**C**) Time-course analysis of GST-NGR5 degradation. HSP90 serves as loading control. (**D**) The degradation rate of His-NGR5 and His-SLR1. (**E**) Tiller number. (**F**, **G**) Relative mRNA abundance and H3K27me3 modification of *D14* (**F**) and *OsSPL14* (**G**). Transcript abundance relative to that of 9311-*sd1* in 1N (set to one). Data shown as mean ± SE (n = 3). (**H**) Natural allelic variation at *NGR5*. (**I**) Tiller number and grain yield. Data shown as mean ± SE (Hap.1, n = 305; Hap.2, n = 84; Hap.3, n = 62; Hap.4, n = 138; Hap.5, n = 97). (**J**) Relative mRNA abundance of *NGR5*. Abundance shown relative to that of *OsActin1*. (**K**) Plant height. Data (**E**, **K**) shown as mean ± SE (n = 20). (**L**, **M**) Grain yield per plot. Data are mean ± SE of six plots (each plot contained 220 plants) per line per nitrogen level. Different letters denote significant differences ($P < 0.05$, panels **E**-**G** and **I**-**M**; Duncan's multiple range test).

Supplementary Figures

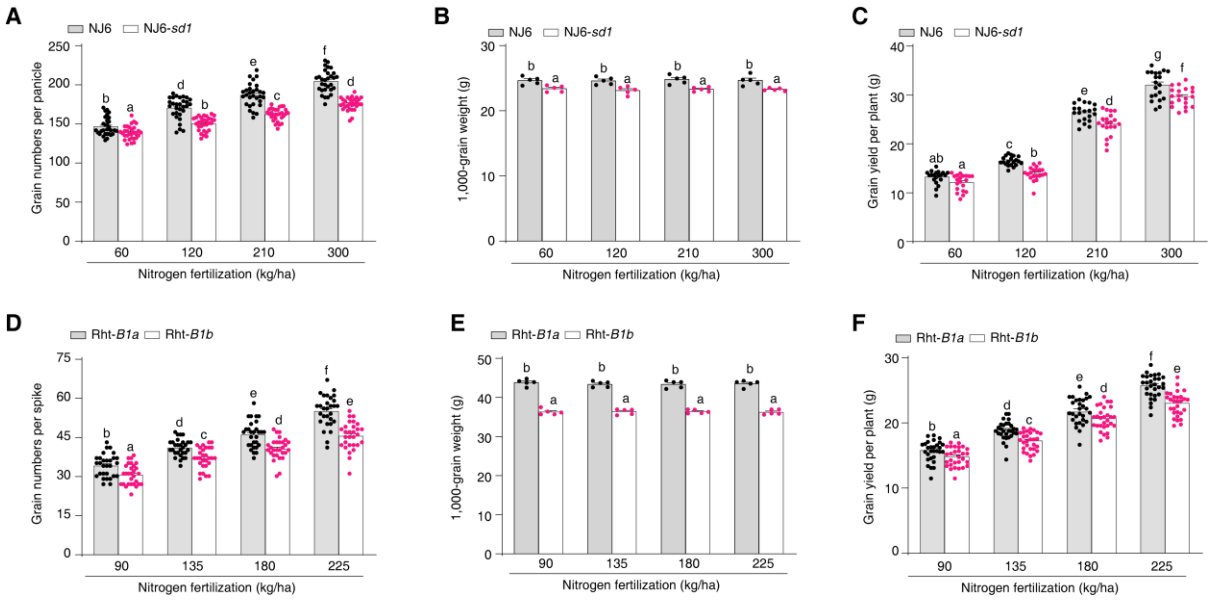

Fig. S1. The effects of the semi-dwarfing genes *sd1* and *Rht-B1b* on agronomic traits of NIL plants grown at varying N supply. (**A**) Rice grain numbers. Data shown as mean ± SE (n = 30). (**B**) Rice 1,000-grain weight. Data shown as mean ± SE (n = 5). (**C**) Rice grain yield. Data shown as mean ± SE (n = 20). (**D**) Wheat grain numbers. Data shown as mean ± SE (n = 30). (**E**) Wheat 1,000-grain weight. Data shown as mean ± SE (n = 5). (**F**) Wheat grain yield. Data shown as mean ± SE (n = 30). Different letters denote significant differences (P < 0.05; Duncan's multiple range test).

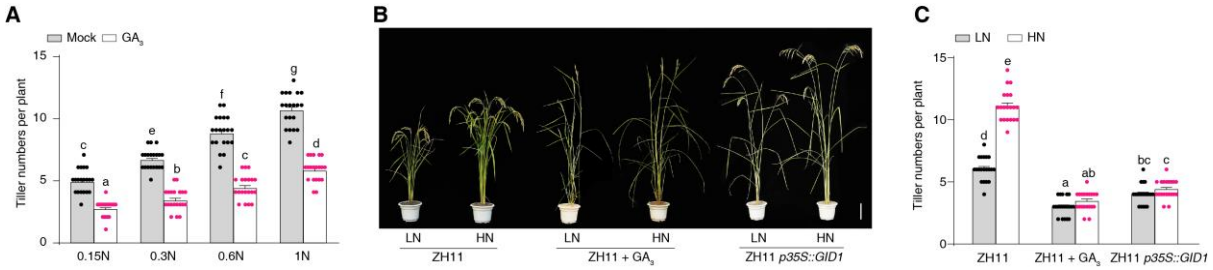

Fig. S2. The GA-GID1 module inhibits rice tiller number. (**A**) The effects of exogenous GA treatment on tillering of *indica* rice GRV 9311 in response to increasing N supply. (**B**) Mature plants grown in low (90 kg/ha; LN) and high (180 kg/ha; HN) N supply with or without 100 μM GA_3 treatment. Scale bar, 20 cm. (**C**) Tiller numbers. Data (**A**, **C**) shown as mean ± SE (n = 20). Different letters denote significant differences (P < 0.05; Duncan's multiple range test).

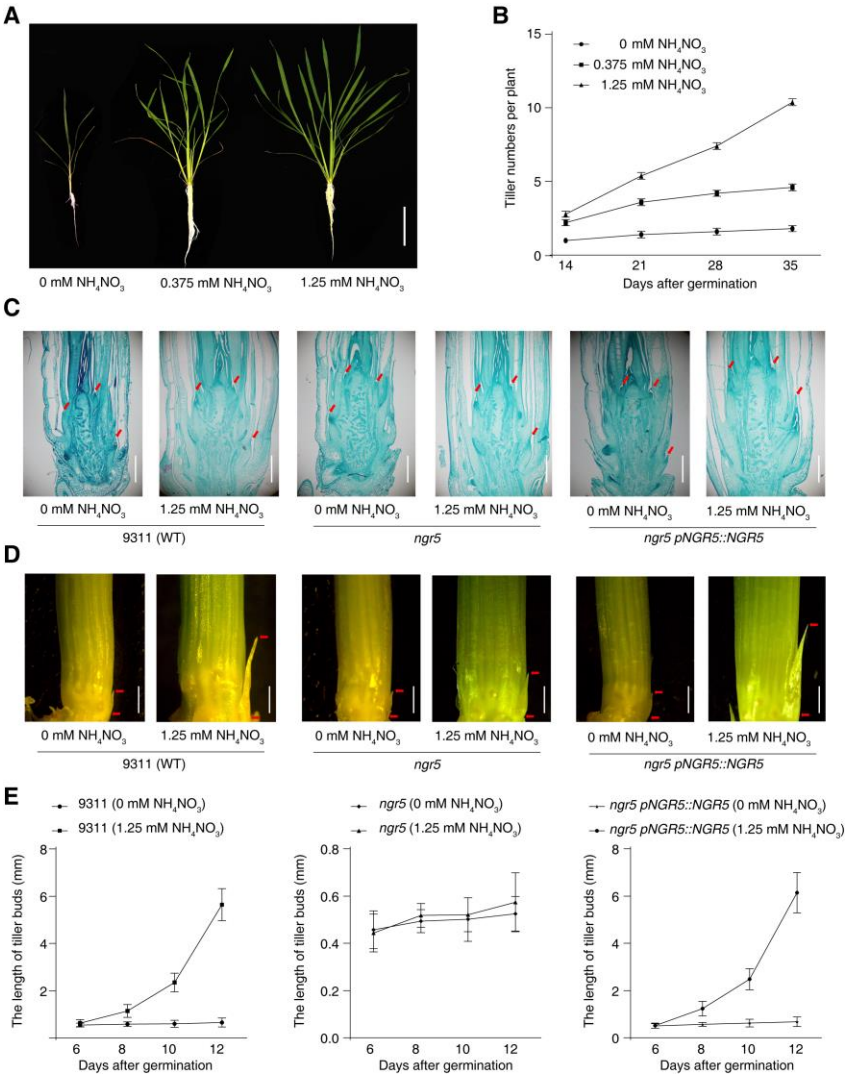

Fig. S3. NGR5 promotes N-dependent outgrowth of tiller buds. (**A**) Increased N enhances plant growth and tillering capacity. Scale bar, 10 cm. (**B**) Tiller number. (**C**) Longitudinal sections of three-leaf stage axils. Arrows indicate axillary meristems. Scale bar, 100 μm. (**D**) Tiller buds of four-leaf stage seedlings. Arrows indicate tiller buds. Scale bar, 2 mm. (**E**) Tiller bud lengths. Data (**B**, **E**) shown as mean ± SE (n = 5).

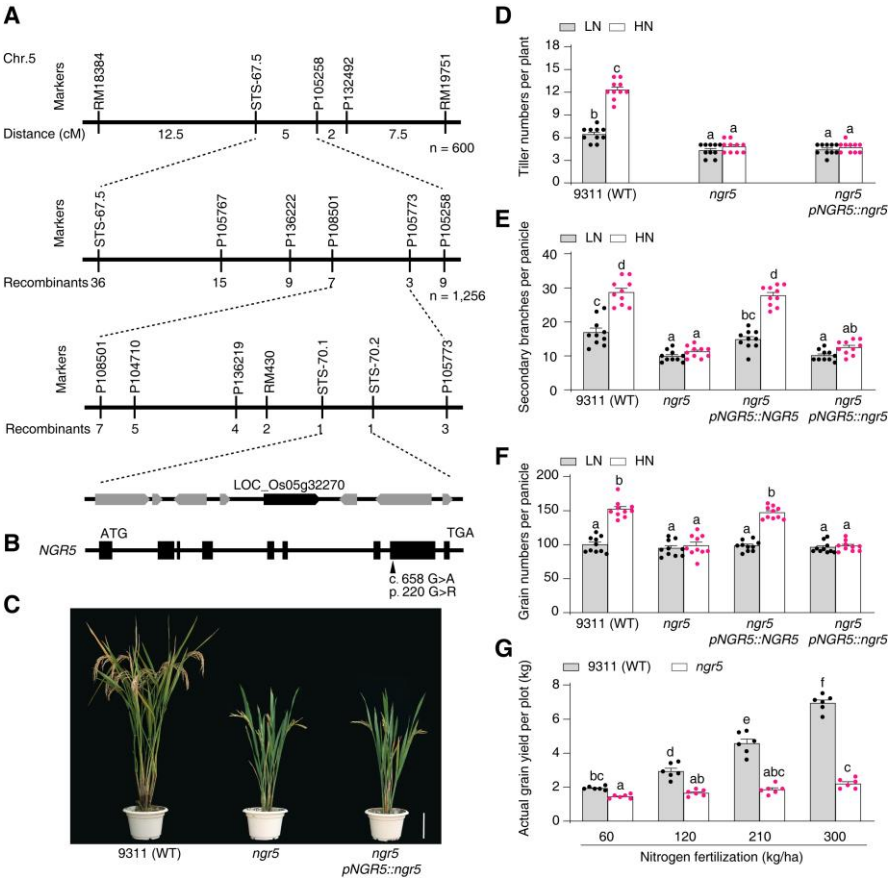

Fig. S4. Positional cloning and genetic complementation of *NGR5*. (**A**) Map-based cloning of *ngr5*. The candidate gene was mapped to a region flanked by molecular marks STS-70.1 and STS-70.2. The numbers below the lines indicate the number of recombinants between *NGR5* and an adjacent marker. The candidate region contains 8 predicted ORFs (open reading frames). (**B**) Sequence variants at the *NGR5* locus. (**C**). Mature plants. Scale bar, 20 cm. (**D**) Tiller numbers per plant. (**E**) Secondary branches per panicle. (**F**) Grain numbers per panicle. The rice plants were grown under low (90 kg/ha; LN) or high (180 kg/ha; HN) N conditions. Data (**D**-**F**) shown as mean ± SE (n = 10). (**G**) Grain yields per plot. Data shown as mean ± SE of six plots (each plot contained 220 plants) per line per N level. Different letters denote significant differences (P < 0.05; Duncan's multiple range test).

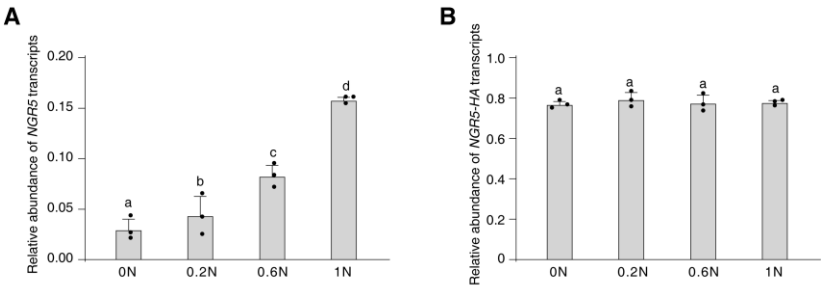

Fig. S5. The effects of N supply on *NGR5* mRNA abundance in transgenic 9311 plants expressing *p35S::NGR5-HA*. (**A**) *NGR5* mRNA abundance (transcribed from endogenous *NGR5* gene). (**B**) *NGR5-HA* mRNA abundance (transcribed from *p35S::NGR5-HA* transgene). All data shown as mean ± SE (n = 3). mRNA abundance shown relative to that of *OsActin1*. Different letters denote significant differences ($P < 0.05$; Duncan's multiple range test).

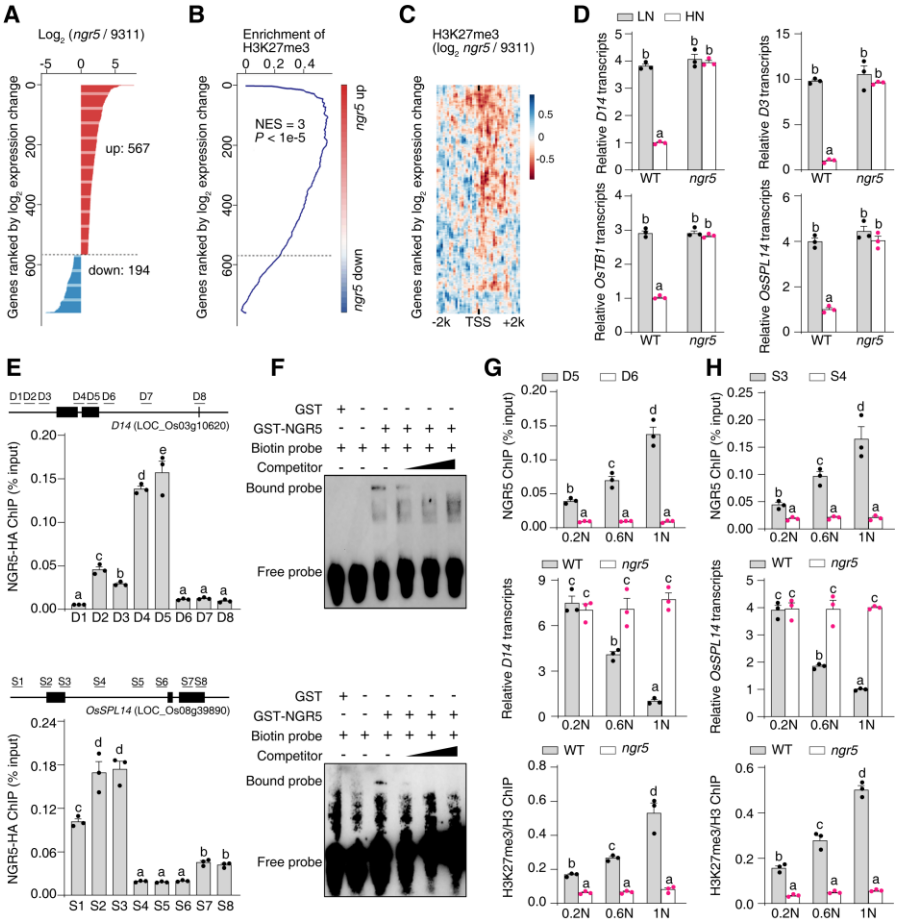

Fig. S6. NGR5 promotes N-dependent repression of shoot branching inhibitor genes. (**A**) Distribution of $\log_2$ fold change for differentially expressed genes, fold change >2; adjusted $P < 0.05$. (**B**) Enrichment of H3K27me3 targets within *NGR5*-repressed genes. (**C**) Log_2 fold change in H3K27me3 levels across TSS (transcription start site) and gene body regions. (**D**) Relative mRNA abundances. (**E**) ChIP-PCR experiments with *D14* and *OsSPL14* (black boxes show protein-encoding ORFs, PCR-amplification of randomly selected regions (D1, S1 etc.) reveals NGR5-HA mediated enrichment (relative to input). (**F**) EMSA assays. DNA fragment D5 or S3 was incubated with GST-NGR5 as indicated. Competition for NGR5 binding was performed with 10×, 20× and 50× unlabelled probes, respectively. (**G**, **H**) ChIP-PCR assays for fragment D5 of *D14* or S3 of *OsSPL14* (D6 and S4 serve as negative controls, respectively) were performed using 3-week-old *pNGR5::NGR5-HA* plants grown in increasing N supply, together with associated analysis of gene expression and H3K27me3 enrichment. mRNA abundance relative to that of WT in 1N (set to one). Data (**D**, **E**, **G** and **H**) shown as mean ± SE ($n = 3$), different letters denote significant differences ($P < 0.05$; Duncan's multiple range test).

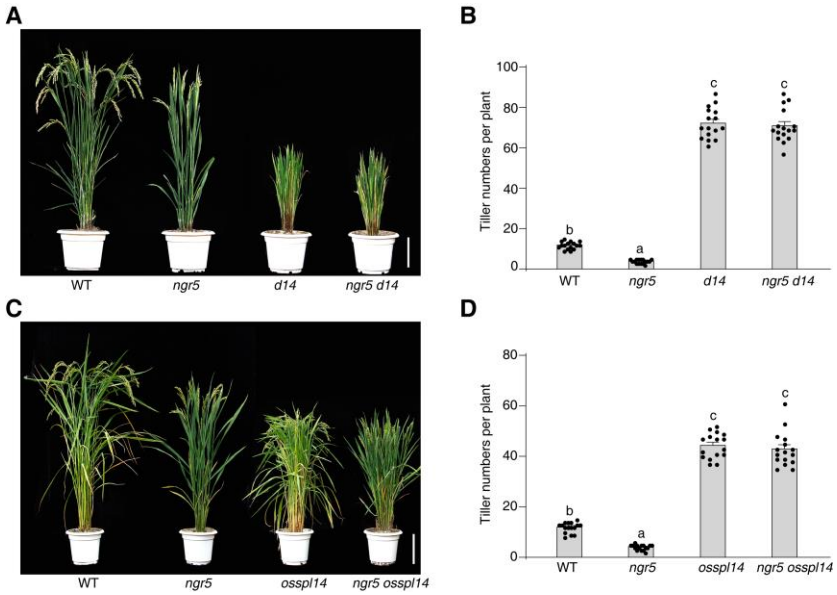

Fig. S7. Shoot branching inhibitor genes *D14* and *OsSPL14* function downstream of *NGR5*. (**A**) Mature plants grown in high (180 kg/ha) N supply. Scale bar, 20 cm. (**B**) Tiller numbers. (**C**) Mature plants grown in high (180 kg/ha) N supply. Scale bar, 20 cm. (**D**) Tiller numbers. Data (**B**, **D**) shown as mean ± SE (n = 16). Different letters denote significant differences ($P < 0.05$; Duncan's multiple range test).

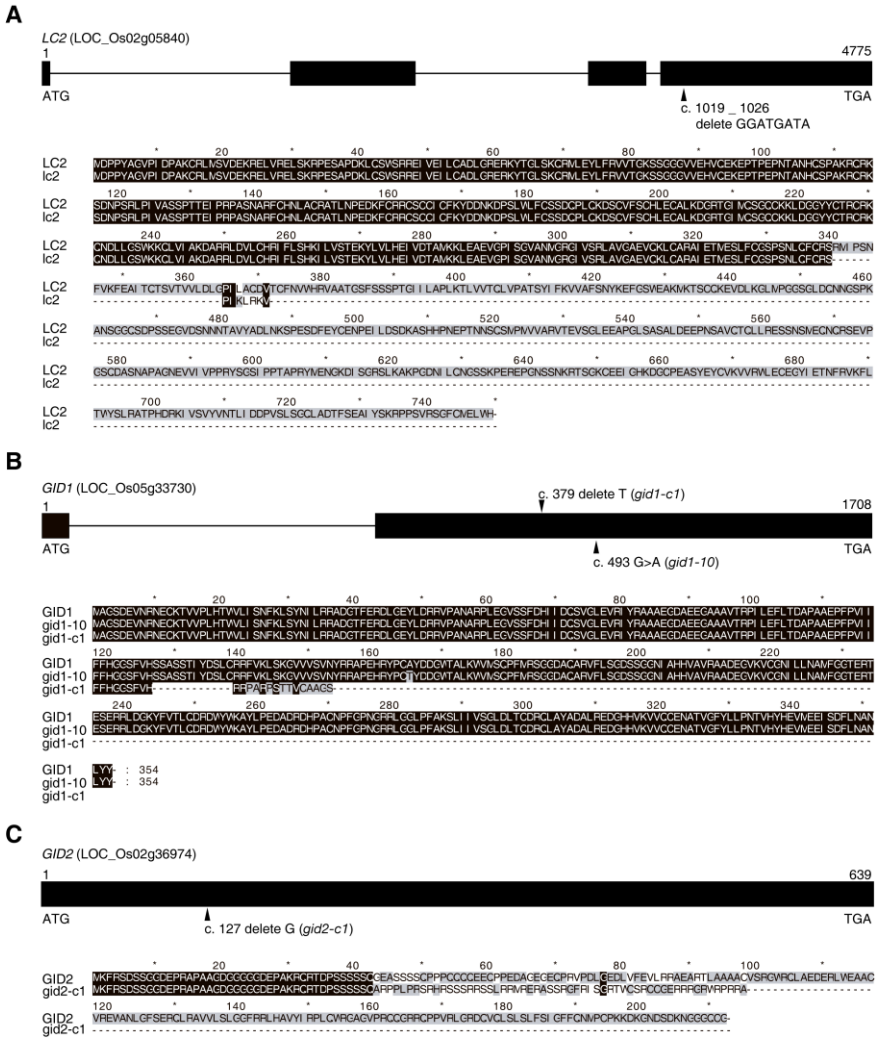

Fig. S8. CRISPR/Cas9-generated gene mutations and predicted protein products. (**A**) *LC2*. (**B**) *GID1*. (**C**) *GID2*. The translational start ATG (nucleotide 1) and closing TGA are shown, together with protein-encoding DNA sequence (CDS, thick black bars). Arrows indicate mutation sites.

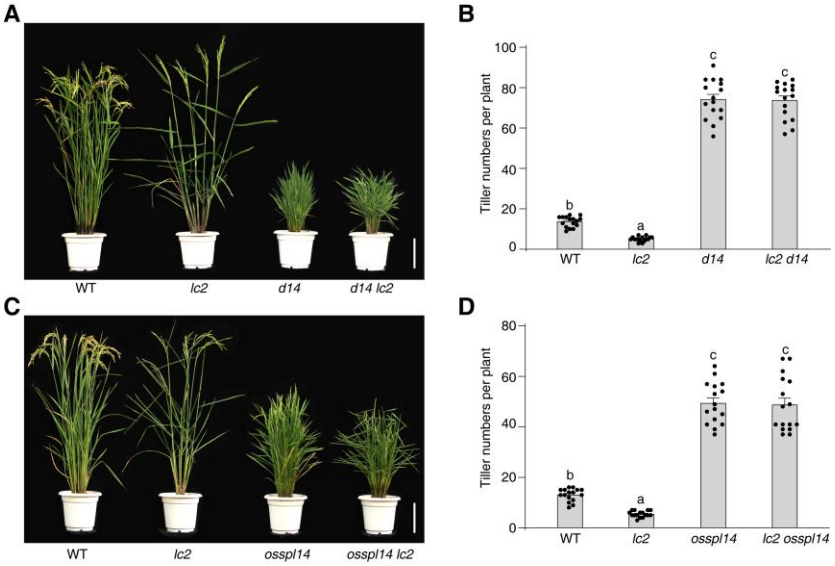

Fig. S9. *D14* and *OsSPL14* mutant alleles are epistatic to *lc2*. (**A**) Mature plants grown in high (180 kg/ha) N supply. Scale bar, 20 cm. (**B**) Tiller number. (**C**) Mature plants grown in high (180 kg/ha) N supply. Scale bar, 20 cm. (**D**) Tiller number. Data (**B**, **D**) shown as mean ± SE (n = 16). Different letters denote significant differences ($P < 0.05$; Duncan's multiple range test).

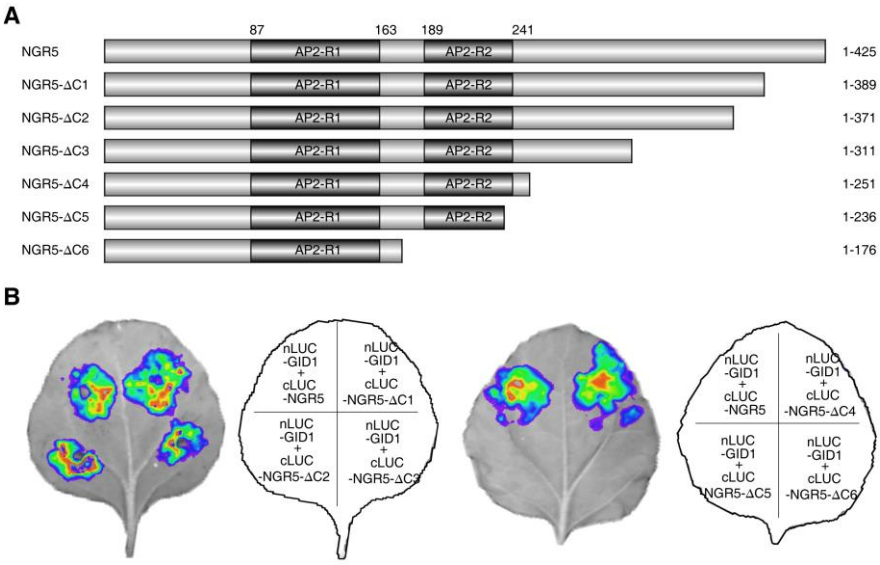

Fig. S10. SFLC visualisation of NGR5-GID1 interaction. (**A**) Schematic representation of the wild-type and mutant truncated NGR5 proteins used for SFLC assays. (**B**) SFLC assays. Constructs expressing wild-type NGR5 and C-terminal deletion variants (shown as in **A**) tagged with the C-terminus of LUC were co-transformed into tobacco leaf epidermal cells, together with constructs expressing GID1 tagged with the N-terminus of LUC, respectively. The pictures of SFLC assays represent one of the three experiments performed independently with similar results.

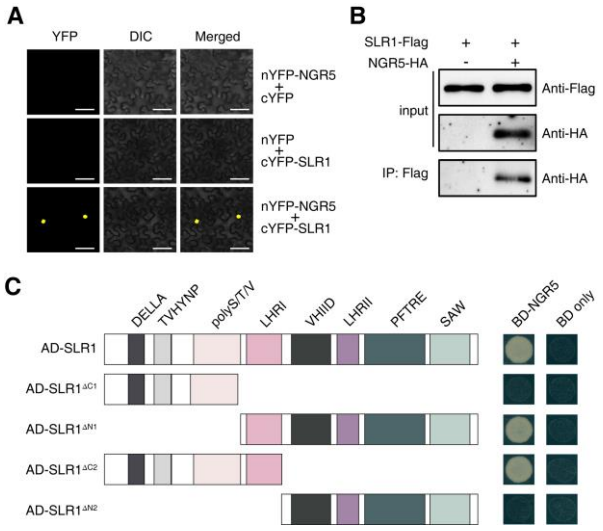

Fig. S11. The LHR1 motif is required for the SLR1-NGR5 interaction. (**A**) BiFC assays. Constructs expressing NGR5 and SLR1 tagged with the N-terminus of YFP were co-transformed into tobacco leaf epidermal cells. Scale bar, 60 μm. (**B**) Co-IP assays. The pictures of BiFC and Co-IP assays represent one of three experiments performed independently with similar results. (**C**) Yeast two-hybrid assays. Schematic representation of the wild-type and mutant truncated SLR1 proteins used for the yeast two-hybrid assay.

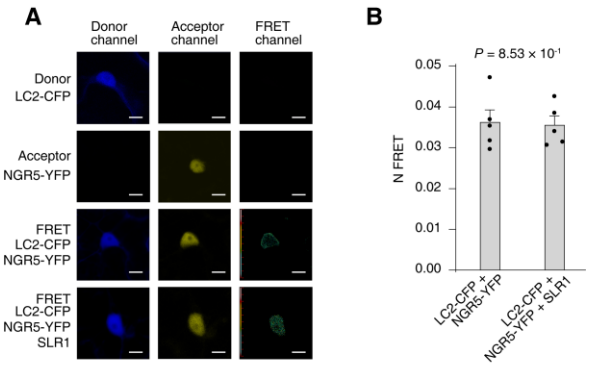

Fig. S12. The effect of SLR1 on the interaction between LC2 and NGR5. (**A**) FRET images. Scale bar, 200 μm. (**B**) Mean N-FRET data for NGR5-LC2 channels. Data shown as mean ± SE (n = 5). A two-sided Student's t-test was used to generate the P values.

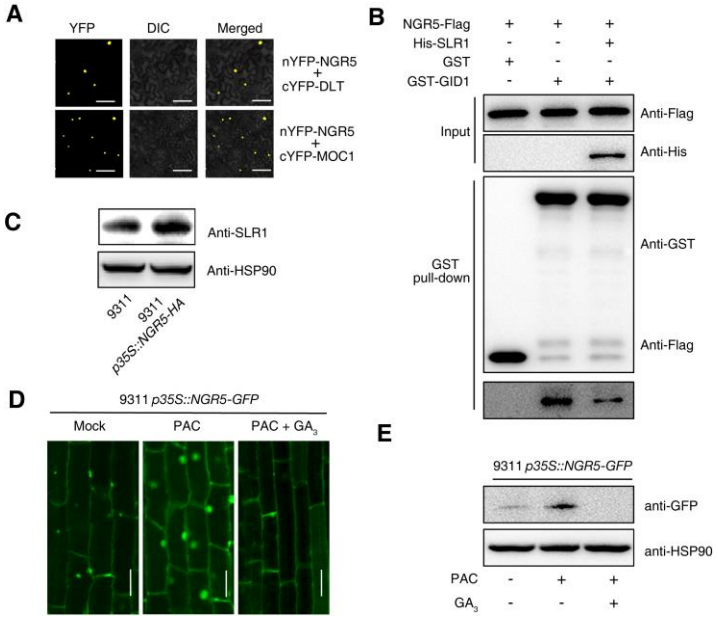

Fig. S13. The effects of SLR1 on GA-mediated degradation of NGR5. (**A**) BiFC assays. Constructs expressing NGR5 tagged with the N-terminus of YFP and GRAS protein (either DLT or MOC1) tagged with the C-terminus of YFP were co-transformed into tobacco leaf epidermal cells. Scale bar, 60 μm. (**B**) Pull-down assays. (**C**) Immunodetection of SLR1. Total proteins were extracted from 3-week-old plants grown at high (180 kg/ha) N supply. HSP90 serves as loading control. (**D**, **E**) Effects of different concentration of GA on NGR5-GFP accumulation. The transgenic rice plants carrying the *p35S::NGR5-GFP* construct were grown on 1/2 MS medium plates containing 2 μM PAC. 3-week-old seedlings were used for analysis of the distribution of GFP in root cells (**D**) and immunodetection of NGR5-GFP (**E**) after 4 h treatment with 1 μM GA_3. HSP90 serves as loading control.

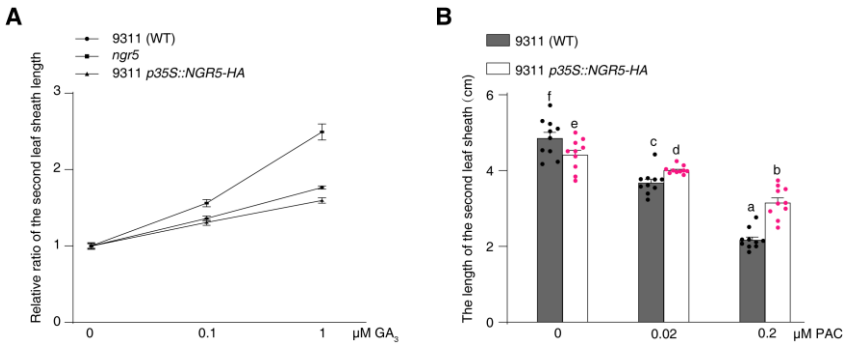

Fig. S14. The effects of *NGR5* on GA-induced growth of the second leaf sheath in rice. (A) Comparison of relative ratio of the second leaf sheath growth among the *ngr5* mutants, transgenic plants carrying the *p35::NGR5-HA* construct and wild-type plants. The length of the second leaf sheath of 10-day-old seedlings grown on 1/2 MS medium without GA treatment is set to one. (**B**) The length of the second leaf sheath of 14-day-old seedlings grown on 1/2 MS medium plates containing various concentrations of PAC. Data shown as mean ± SE (n = 10). Different letters denote significant differences ($P < 0.05$; Duncan's multiple range test).

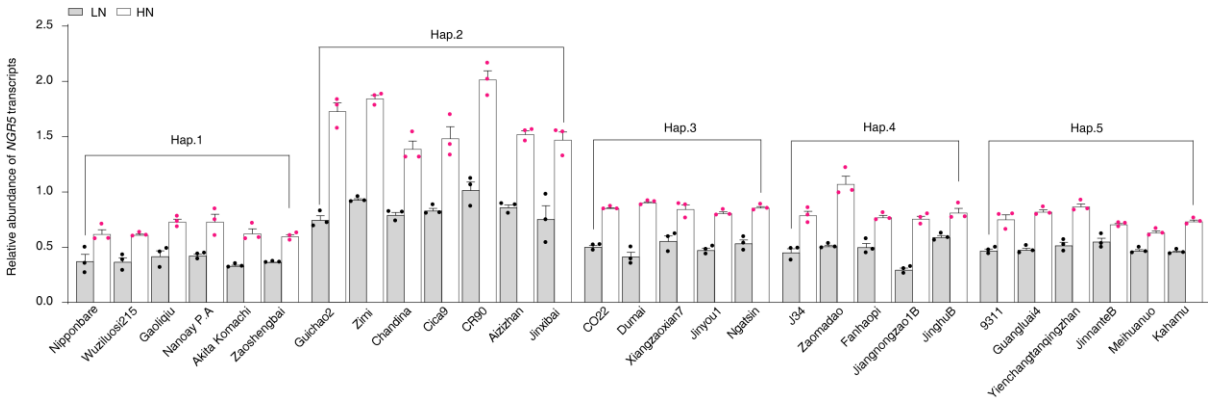

Fig. S15. Relative abundance of *NGR5* mRNA in tiller buds. Comparisons of *NGR5* mRNA abundance in tiller buds of 3-week-old plants grown in high (HN, 1.25 mM NH_4NO_3) or low (LN, 0.25 mM NH_4NO_3) N conditions. Data shown as mean ± SE (n = 3). mRNA abundance shown relative to that of *OsActin1*.